

Vibrational density of states of silicon nanoparticles

R. Meyer^{1,*} and D. Comtesse²

¹*Department of Mathematics and Computer Science, Laurentian University,
935 Ramsey Lake Road, Sudbury (Ontario) P3E 2C6, Canada*

²*Fachbereich Physik, Universität Duisburg-Essen, Lotharstraße 1, D-47048 Duisburg, Germany*
(Submitted to Phys. Rev. B: June 1, 2019)

The vibrational density of states of silicon nanoparticles in the range from 2.3 to 10.3 nm is studied with the help of molecular-dynamics simulations. From these simulations the vibrational density of states and frequencies of bulk-like vibrational modes at high-symmetry points of the Brillouin-zone have been derived. The results show an increase of the density of states at low frequencies and a transfer of modes from the high-frequency end of the spectrum to the intermediate range. At the same time the peak of transverse optical modes is shifted to higher frequencies. These observations are in line with previous simulation studies of metallic nanoparticles and they provide an explanation for a previously observed discrepancy between experimental and theoretical data [C. Meier *et al.*, Physica E, **32**, 155 (2006)].

PACS numbers: 63.22.Kn,62.25.Jk,81.05.Cy,02.70.Ns

I. INTRODUCTION

Modern nanotechnology is leading to the development of a new generation of applications and devices based on nanostructured materials. An important part of the development of many nano-devices is the thermal design. If the heat generated inside a device cannot be transported away efficiently, the system will fail or even break due to overheating. Thermal properties like heat capacity and thermal conductivity as well as many other material properties are strongly influenced by the vibrational density of states (VDOS). For this reason a profound understanding of the laws governing the vibrational properties of nanostructured materials is of high technological and fundamental interest.

This article focuses on the vibrational properties of silicon nanoparticles. Silicon is an important engineering material whose bulk properties have been studied extensively. Its favourable electrical properties have made it the base material for all microelectronics and advanced technology exists for the manufacturing of nanostructured silicon based devices.

The vibrational properties of bulk crystalline Si have been studied both experimentally using neutron scattering techniques^{1,2} as well as theoretically using empirical and first-principles methods.³⁻⁵ In addition to this, Raman scattering experiments have been used in numerous studies of the vibrational properties of silicon nanostructures.⁶⁻¹⁶ In many of these studies it is found that the first order peak due to the transverse optical (TO) phonon at the Γ point is broadened and its maximum shifted to lower energies. The phonon-confinement model^{6,17} attributes this behaviour to the fact that in nanostructures more vibrational modes can become Raman active than in bulk crystals since the translational symmetry is broken and consequently no $\Delta\mathbf{k} = 0$ selection rule applies. In Ref. 15, Meier et al. observed pronounced decreases of the Raman shift in Silicon nanoparticles. A comparison with calculated values based on

the phonon-confinement model showed the experimentally observed decrease of the Raman shift to be considerably stronger than predicted by the model calculations.¹⁵

Theoretically, the vibrational properties of nanostructured silicon have also been studied. Heino has calculated phonon dispersion relations for silicon thin films using molecular-dynamics simulations¹⁸ whereas Saviot *et al.* have studied low frequency vibrational modes in silicon nanoparticles using an elastic continuum model.¹³ Hu *et al.* and Valentin *et al.* employed empirical atomistic force models to calculate the VDOS of silicon nanoparticles by diagonalization of the dynamical-matrix.^{19,20} The latter two studies did not include relaxation effects from the particle surfaces.

In this work, we use molecular-dynamics simulations in combination with the modified embedded-Atom method (MEAM)^{21,22} potential for silicon from Ref. [23] to calculate the vibrational density of states and selected zone-boundary phonon frequencies for silicon nanoparticles with diameters in the range 2.3 – 10.3 nm. These simulations include surface effects and the results show changes from the bulk density of states that are similar to those observed in metallic nanoparticles.²⁴⁻²⁷ While the limitations of the potential do not allow us to make quantitative predictions, our calculations show clear trends in the development of the particle VDOS as the particle size is reduced. In particular, we observe an increase of the VDOS at low frequencies, a shift of the high frequency modes to higher frequencies and a transfer of weight from the TO mode peak to intermediate frequencies. Our results provide an explanation for the discrepancy observed in Ref. 15.

II. COMPUTATIONAL DETAILS

The calculations of vibrational properties of Si nanoparticles presented in this work are all based on molecular-dynamics simulations using the MEAM poten-

TABLE I: Approximate diameters d of the model particles and the number of atoms N they contain.

	4.1	6.1	8.2	10.3
N	329	657	1803	5815
				14175
				27943

tial for Si from Ref. 23. The advantage of the MEAM formalism^{21,22} is that it is not only suitable for simulations of pure Si in the diamond structure but that it has also been used successfully in studies of composite systems combining Si with other elements like, Ni,²³ Mb,²⁸ or Au.²⁹ A disadvantage of the potential is that it severely overestimates the phonon frequencies in silicon.¹⁸ Qualitatively the potential gives however a fair description of silicon and reflects the characteristic features of its phonon dispersion relations. Since in this work we are more interested in the qualitative changes of the VDOS than quantitatively exact frequencies and since we hope to exploit the potential's transferability in future work focusing on composite systems, we decided to use this potential despite its shortcomings.

In order to study the influence of particle size on the vibrational properties in Si nanoparticles, we constructed a set of model particles by cutting a spherical region out of an ideal diamond lattice. The diameters of the particles and the number of atoms they contain are summarized in Table I. In addition to the nanoparticle configurations we used a bulk-like configuration containing 1,000,000 Si atoms arranged on an ideal $50 \times 50 \times 50$ cells diamond lattice.

Prior to the calculation of vibrational frequencies, we carefully equilibrated our model systems at $T = 300$ K. In order to determine the equilibrium lattice constant of the bulk configuration at this temperature, the Parinello-Rahman technique was employed to perform simulations at constant pressure ($p = 0$). After the determination of the lattice constant, the configuration was re-equilibrated with a fixed volume. All simulations were carried out using the velocity Verlet algorithm with a time step $\Delta t = 0.5$ fs. In simulations of the bulk configuration, periodic boundary conditions were applied.

For the calculations of vibrational properties from our simulations we relied on the velocity-autocorrelation function. The total VDOS $g(\nu)$ of a system of particles is proportional to the Fourier-transform of the velocity-autocorrelation function averaged over all particles. The normalized VDOS of an N particle system is thus given by

$$g(\nu) = \int_{-\infty}^{\infty} dt \frac{\sum_{i=1}^N \langle \mathbf{v}_i(t) | \mathbf{v}_i(0) \rangle}{\sum_{i=1}^N \langle \mathbf{v}_i(0) | \mathbf{v}_i(0) \rangle} e^{i2\pi\nu t} \quad (1)$$

where \mathbf{v}_i denotes the velocity of the i -th particle. Information about individual vibrational frequencies can be obtained by this method if the velocities of the particles are projected onto a plane wave.

For a mode with wave-vector \mathbf{q} and a normalized po-

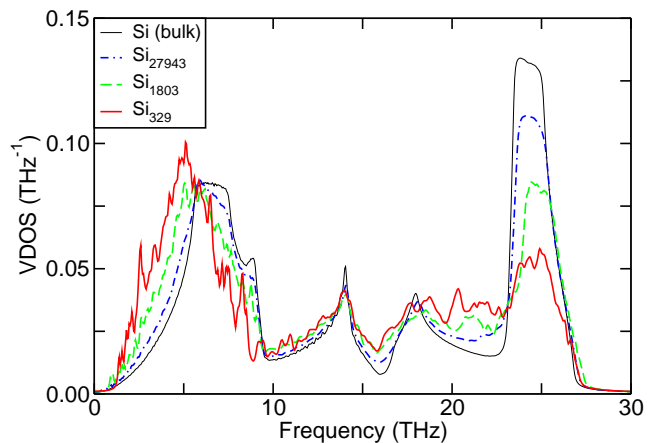


FIG. 1: (Color online) Normalized vibrational density of states of crystalline bulk Si and nanoparticles of various sizes. The data have been broadened with a finite line-width of corresponding to an energy of ≈ 0.12 THz

larization vector \mathbf{p} we calculated the function

$$g_{\mathbf{q}}^p(\nu) = \int_{-\infty}^{\infty} dt \frac{\langle v_{\mathbf{q}}^p(t) | v_{\mathbf{q}}^p(0) \rangle}{\langle v_{\mathbf{q}}^p(0) | v_{\mathbf{q}}^p(0) \rangle} e^{i2\pi\nu t} \quad (2)$$

where

$$v_{\mathbf{q}}^p(t) = \sum_{i=1}^N \mathbf{p} \cdot \mathbf{v}_i(t) e^{-i\mathbf{q} \cdot \mathbf{r}_i^0} \quad (3)$$

is the projection of the velocities on the plane wave and \mathbf{r}_i^0 denotes the average position of the i -th particle. For a crystalline system with translational symmetry the function $g_{\mathbf{q}}^p$ should have sharp peaks at the positions of the phonons with wave-vector \mathbf{q} that have a component along the polarization vector \mathbf{p} .

The vibrational modes of systems without translational symmetry are not plane waves. For systems similar to perfect crystals (for example a finite piece cut out of an infinite crystal) one finds however that the vibrational modes are well described by phonon-like wave-packets. Such wave-packets appear in $g_{\mathbf{q}}^p(\nu)$ as more or less broadened peaks whose maxima can still be used to determine the dominant frequency of the mode. The quality of the peaks in $g_{\mathbf{q}}(\nu)$ — if there are clear, isolated peaks — can therefore be used to judge to what extent the phonon picture applies to the system in question.

III. RESULTS

In Fig. 1 we compare the VDOS that we obtained for three selected nanoparticles with the result of crystalline bulk Si. Since for the smaller particles the discrete nature of the spectrum becomes notable, we have broadened the VDOS data with a finite line-width corresponding to an energy of 0.5 meV (0.12 THz). As observed previously in Ref. 18, the MEAM potential from Ref. 23

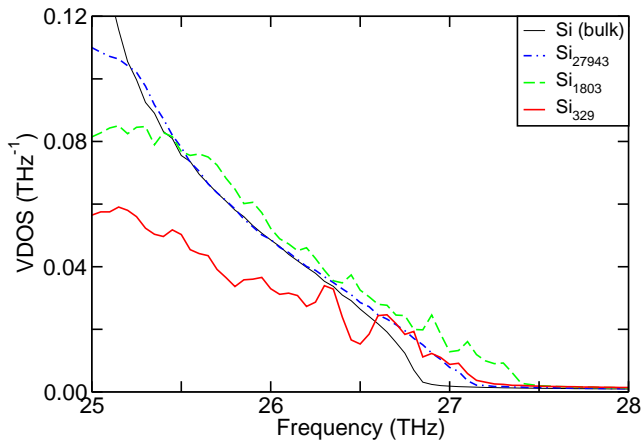


FIG. 2: (Color online) High frequency part of the normalized vibrational density of crystalline bulk Si and nanoparticles of various sizes.

leads quantitatively to strongly exaggerated phonon frequencies. Qualitatively however, the results show a clear evolution of the VDOS as the particle size is diminished with the strongest changes occurring at the upper and lower end of the frequency spectrum.

It can be seen from Fig. 1 that with decreasing particle size the large peak of transverse acoustic (TA) modes in the range 0 – 10 THz is shifted to lower frequencies. The resulting increase of the VDOS is further amplified by the fact that the curves become more linear for the smaller particles. These two changes lead together to a significant increase of the low-frequency VDOS. There is however no notable loss of the height of the TA mode peak.

In the high-frequency range the VDOS of the Si nanoparticles show a different behavior. As shown by Fig. 1, the strong peak of the TO modes around 25 THz loses its height rapidly with increasing particle size without a significant increase in peak width. In addition to this, the TO peak is slightly shifted to higher frequencies. This can also be seen in Fig. 2 where we show the high frequency flank of the TO peak without line broadening. This figure makes it clear that for the nanoparticle systems this flank of the peak and the cutoff frequency are located at higher frequencies than in the bulk system. Due to the lower peak height the VDOS curves of the particles eventually cross the bulk line at frequencies between 25 and 26.5 THz but it is clear from Fig. 1 that this is not due to a peak broadening but a shift to higher frequencies. The shift of the TO peak will be discussed in more detail below by looking at the frequencies of individual vibrational modes.

Interestingly we observe a non-monotonous behavior of the cut-off frequencies as shown by the fact that the cut-off frequencies of the Si_{329} and Si_{27943} particles are both lower than that of Si_{1803} . We interpret this as an indication that our smallest particles are below the limit of the scaling regime in which the physical properties scale

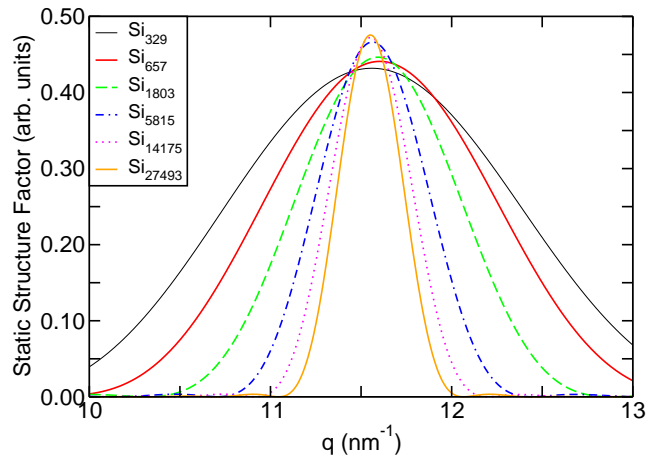


FIG. 3: (Color online) Static structure factor along the line $\mathbf{q} = [qqq]$ for Si nanoparticles of various sizes.

monotonously with the particle size in a simple manner. This view is confirmed by other results discussed below.

At intermediate frequencies, the VDOS data presented in Fig. 1 show only little differences between the nanoparticles and the bulk system. In particular, the shape and the position of the longitudinal acoustic (LA) modes peak at approximately 14 THz remains remarkably constant for all of our model systems. On the other hand, the position of the longitudinal optical (LO) mode peak at 18 THz is slightly shifted to higher frequencies. In the regions to the left and to the right of the LO peak the VDOS increases with decreasing particle sizes. This increase accounts obviously for the loss of weight in the TO peak.

From metallic nanoparticles it is known that the curved surface of nanoparticles gives rise to a capillary pressure which affects the lattice constant inside the particles (see e.g. Ref. 26). In order to perform calculations of individual vibrational modes at high-symmetry points of the Brillouin zone, it was therefore necessary for us to determine the lattice constants of the equilibrated model nanoparticles. In order to do so, we calculated the static structure factor of the model particles and obtained the lattice constant from the position of the (111) peak.

Figure 3 shows the static structure factor along the [111] direction for all of our model particles. Except for the smallest particle, the maximum of the (111) peak shifts to larger values of q with decreasing particle size. This is the expected behavior since the smaller particles should have a larger capillary pressure (assuming a positive surface stress for Si) and consequently a smaller lattice constant. The fact that the position of the maximum of the Si_{329} particle moves against the trend is another indication that this particle is outside the scaling regime for Si particles. It should be understood here that the lattice constants derived from q_{max} are only meant to be used as approximate, average values since the crystal lattice in the nanoparticles is not homogenous. Capillary pressure compresses the lattice inside the particles

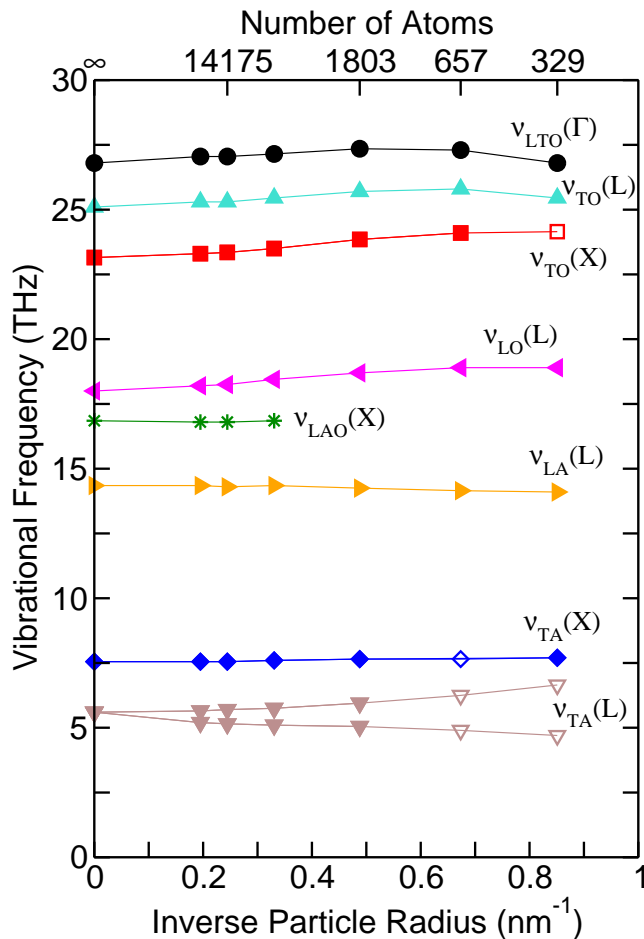


FIG. 4: (Color online) Frequencies of selected Si nanoparticle phonon modes as a function of the inverse particle radius. Data at $1/R = 0 \text{ nm}^{-1}$ represent crystalline bulk values. For further discussions see main article text.

whereas the surface stress has the inverse effect in the vicinity of the surface.

With the average lattice constants derived from the static structure factor calculations, we calculated the frequencies of the vibrational modes corresponding to the Γ , X, and L point of the Brillouin-zone of the diamond lattice for all of our model nanoparticles using the method outlined in Sec. II. The frequencies obtained from the maxima of the peaks in the projected density of states $g_{\mathbf{q}}^p(\nu)$ are presented in Fig. 4. Note that at the Γ point the LO and TO modes and at the X point the LA and LO modes are degenerate. For this reason the frequencies of these modes are denoted by $\nu_{LTO}(\Gamma)$ and $\nu_{LAO}(X)$, respectively.

For the larger particles and the bulk system the analysis procedure gave straightforward, unambiguous results indicating that the vibrational modes are sufficiently similar to plane waves. In case of the smaller particles Si_{329} and Si_{657} , however, the projected density of states sometimes showed a group of similar peaks instead of a single peak. If in such a case it was still possible to identify one

peak that was clearly most consistent with the rest of the data we marked the corresponding data point with an open symbol in Fig. 4. In the case of the $\nu_{LAO}(X)$ mode, however, it turned out to be impossible to identify matching peaks for all particles smaller than Si_{5815} so that these points were dropped from the figure.

A special case is the $\nu_{TA}(L)$ mode. For this mode, the projected density of states of all nanoparticles showed two clearly distinguishable peaks. This indicates that the degeneracy of this mode is lifted in the finite particles. For this reason we included two distinct data sets for this mode in Fig. 4.

The behavior of the individual frequencies is generally consistent with the changes in the total density of states shown in Fig. 1. In the bulk system, the TA modes at the L and X point define the upper and lower boundary of the flat plateau on top of the TA peak. The broadening and shift of this peak in the total VDOS compares well with the fact that $\nu_{TA}(X)$ remains nearly constant, whereas the lower branch of the L-point TA mode shifts to lower frequencies for smaller particles.

In the intermediate frequency regime, the sharp maxima of the LA and LO mode peaks correspond to $\nu_{LA}(L)$ and $\nu_{LO}(L)$ in the bulk case. Again, the very small shift of $\nu_{LA}(L)$ and the slightly stronger upward shift of $\nu_{LO}(L)$ compare well with the changes in the total VDOS. This indicates that these modes are well described by the bulk-phonon picture.

At high frequencies, $\nu_{TO}(X)$ and $\nu_{TO}(L)$ correspond to the lower and upper bound of the TO peak in the bulk case, whereas $\nu_{LTO}(\Gamma)$ defines the cut-off frequency. The general increase of these frequencies with decreasing particle size (except for Si_{329}) reflects the shift of the TO peak and the cut-off point in the same direction as shown in Fig. 1 and 2. Moreover, the data in Fig. 4 support a slight sharpening of the TO peak; however the diminishing height of this peak in the VDOS makes it hard to verify this in Fig. 1. The slight decrease of the TO mode frequencies in the case of the smallest particle gives further evidence of the growing deviations from the bulk behavior in particles with diameters below 3 nm.

Although the general trends of Fig. 4 agree well with the behavior of the VDOS, one has to be careful not to stretch these comparisons too far. As pointed out in the last paragraph, $\nu_{LTO}(\Gamma)$ represents the cutoff frequency in the bulk case. In case of Si_{329} , however, the calculated value of $\nu_{LTO}(\Gamma) = 26.80 \text{ THz}$ is the same as in the bulk case, although Fig. 2 clearly shows that modes with higher frequencies are present in this cluster. This discrepancy is another hint that this particle is close to the limit of the regime where the phonon picture can be applied successfully.

IV. SUMMARY AND CONCLUSIONS

We have studied the vibrational properties of silicon nanoparticles with diameters in the range 2.3-10.3 nm us-

ing molecular-dynamics simulations. Our results show clear changes of the VDOS as the particles become smaller. The strongest changes are visible in the low- and high-frequency part of the spectrum. At low frequencies, the VDOS increases as the particles become smaller and the TA mode peak is shifted to lower energies whereas at the upper end of the spectrum, the height of the TO mode peak is significantly reduced although the peak is shifted slightly (< 1 THz) to higher frequencies.

The observed changes of the VDOS can have two reasons. On the one hand, the finite size of the nanoparticles gives rise to vibrational surface modes that are not present in the bulk crystal. On the other hand, the change of boundary conditions at the surface, as well as structural relaxations can modify the frequency of bulk-like modes without affecting their phonon-like nature.

Our calculations of the frequencies of individual vibrational modes make it possible to shed some light on the reasons that are responsible for the observed VDOS changes. As shown in Fig. 4 the TO phonon modes are shifted to higher frequencies. This shift is most likely caused by the capillary pressure which compresses and stiffens the lattice inside the particles. Since the shift of the TO modes appears to affect all TO modes rather homogeneously, the presence of capillary pressure explains the shift of the TO peaks in Fig. 1. The shift of the bulk-like phonon modes to higher frequencies is however contrary to the transfer of weight from the TO peak to intermediate frequencies. We therefore attribute this transfer to the appearance of surface modes.

The increase of the VDOS at intermediate frequencies around 20 THz at the expense of the height of the TO mode peak provides a good explanation for the experimentally observed decrease of Raman shifts in silicon nanoparticles.¹⁵ Calculations of Meier *et al.*¹⁵ have shown that the measured Raman frequencies are lower than those predicted by the phonon confinement model. Their calculations, however, used the dispersion relations of bulk silicon and did not include any changes of the VDOS in the nanoparticles. We therefore conclude that the strong transfer of weight from the TO peak to lower frequencies in our simulations can account for the observed discrepancy between the experimental results and the phonon confinement model.

At low frequencies the situation is more complicated. Figure 4 shows that some of the TA modes are nearly unaffected by the particle size whereas the TA mode at the L point is split into two modes that move into opposite directions. Although these changes of the bulk-like modes certainly contribute to the shift and change of structure of the TA peak, it is unlikely that the changes of bulk-like modes are the main reason for the dramatic increase of the left flank of the TA peak around 2.5 THz. This in-

crease which goes hand in hand with the transition to a more linear increase is probably caused by low-frequency surface modes.

In general, our calculations agree well with previous studies of the vibrational properties of fcc and bcc metal nanoparticles.^{24,26,27,30,31} Similar to the observations in this study, the metal nanoparticles show an increase and more linear behavior of the VDOS at low frequencies whereas the high frequency LA peak (note that there are no optical modes in the fcc and bcc lattices) is diminished and shifted to higher frequencies. Partial density of states calculations have shown that the increase of the low-frequency VDOS and the loss of weight of the LA peak in copper nanoparticles can be attributed to modes localized at the particle surfaces^{26,27} whereas the shift of the LA peak is caused by capillary pressure.^{25,26}

The structure of the calculated VDOS and the fact that we were able to derive phonon frequencies from the projected density of states shows that the phonon picture can be successfully used to describe the vibrational modes in Si nanoparticles with diameters down to sizes below 4 nm. For particles with diameters of 3 nm and less our results indicate an onset of non-monotonous changes of physical properties as a function of the particle size. This means that the size of these particles is below the lower limit of the scaling regime where properties scale with the particle diameter in a simple manner. The vibrational modes of particles in this range are still rather bulk-like, but deviations from the bulk picture become more pronounced. This finding agrees with Ref. 20 where it was concluded that for silicon particles with diameters above 2.5 nm the VDOS becomes bulk-like.

Unfortunately, the limitations of the MEAM potential employed in this work do not allow calculations of quantitatively correct phonon frequencies. For this reason it would be interesting to verify our results with another model. While DFT calculations of the larger particles are currently out of reach, it might be possible to perform such calculations for the smallest particles used in this study.

Acknowledgments

R.M. would like to thank A. Lorke and C. Meier for fruitful discussions and insight into their experimental results. We also thank P. Entel for his discussions about our simulations. Support by the Shared Hierarchical Academic Research Network (SHARCNET)³² and the *Deutsche Forschungsgemeinschaft* (SFB 445) is gratefully acknowledged.

* Electronic address: rmeyer@cs.laurentian.ca

¹ G. Dolling, in *Inelastic Scattering of Neutrons in Solids*

- and *Liquids*, edited by S. Eklund (International Atomic Energy Agency, Vienna, 1963), vol. II.
- ² G. Nilsson and G. Nelin, *Phys. Rev. B* **6**, 3777 (1972).
 - ³ B. P. Pandey and B. Dayal, *J. Phys. C: Solid State Phys.* **6**, 2943 (1973).
 - ⁴ P. Giannozzi, S. de Gironcoli, P. Pavone, and S. Baroni, *Phys. Rev. B* **43**, 7231 (1991).
 - ⁵ S. Wei and M. Y. Chou, *Phys. Rev. B* **50**, 2221 (1994).
 - ⁶ H. Richter, Z. P. Wang, and L. Ley, *Solid State Comm.* **39**, 625 (1981).
 - ⁷ S. Furukawa and T. Miyasato, *Phys. Rev. B* **38**, 5726 (1988).
 - ⁸ Z. Sui, P. P. Leong, I. P. Herman, G. S. Higashi, and H. Temkin, *Appl. Phys. Lett.* **60**, 2086 (1992).
 - ⁹ H. Mündler, C. Andrzejak, M. G. Berger, U. Klemradt, H. Lüth, R. Herino, and M. Ligeon, *Thin Solid Films* **227**, 27 (1992).
 - ¹⁰ M. Fujii, Y. Kanzawa, S. Hayashi, and K. Yamamoto, *Phys. Rev. B* **54**, R8373 (1996).
 - ¹¹ H. Tanino, A. Kuprin, H. Deai, and N. Koshida, *Phys. Rev. B* **53**, 1937 (1996).
 - ¹² N. Wang, Y. Tang, Y. Zhang, C. Lee, I. Bello, and S. Lee, *Chem. Phys. Lett.* **299**, 237 (1999).
 - ¹³ L. Saviot, D. B. Murray, and M. C. Marco de Lucas, *Phys. Rev. B* **69**, 113402 (2004).
 - ¹⁴ K. W. Adu, H. R. Gutiérrez, U. J. Kim, G. U. Sumanasekera, and P. C. Eklund, *Nano Lett.* **5**, 409 (2005).
 - ¹⁵ C. Meier, S. Lüttjohann, V. Kravets, H. Nienhaus, A. Lorke, and H. Wiggers, *Physica E* **32**, 155 (2006).
 - ¹⁶ D. Ristić, M. Ivanda, and K. Furić, *J. Mol. Struct.* **924**–**926**, 291 (2009).
 - ¹⁷ I. H. Campbell and P. M. Fauchet, *Solid State Comm.* **58**, 739 (1986).
 - ¹⁸ P. Heino, *Eur. Phys. J. B* **60**, 171 (2007).
 - ¹⁹ X. Hu, G. Wang, W. Wu, P. Jiang, and J. Zi, *J. Phys.: Condens. Matter* **13**, L835 (2001).
 - ²⁰ A. Valentin, J. Sée, S. Galdin-Retailleau, and P. Dollfus, *J. Phys.: Conf. Ser.* **92**, 012048 (2007).
 - ²¹ M. I. Baskes, J. S. Nelson, and A. F. Wright, *Phys. Rev. B* **40**, 6085 (1989).
 - ²² M. I. Baskes, *Phys. Rev. B* **46**, 2727 (1992).
 - ²³ M. I. Baskes, J. E. Angelo, and C. L. Bisson, *Modelling Simul. Mater. Sci. Eng.* **2**, 505 (1994).
 - ²⁴ A. Kara and T. S. Rahman, *Phys. Rev. Lett.* **81**, 1453 (1998).
 - ²⁵ R. Meyer, S. Prakash, and P. Entel, *Phase Transitions* **75**, 51 (2002).
 - ²⁶ R. Meyer, L. J. Lewis, S. Prakash, and P. Entel, *Phys. Rev. B* **68**, 104303 (2003).
 - ²⁷ R. Meyer and P. Entel, *Z. Kristallogr.* **222**, 646 (2007).
 - ²⁸ M. I. Baskes, *Mater. Sci. Eng.* **A261**, 165 (1999).
 - ²⁹ C.-L. Kuo and P. Clancy, *Surface Sciences* **551**, 39 (2004).
 - ³⁰ D. Y. Sun, X. G. Gong, and X.-Q. Wang, *Phys. Rev. B* **63**, 193412 (2001).
 - ³¹ B. Roldan Cuenya, A. Naitabdi, J. Croy, W. Sturhahn, J. Y. Zhao, E. E. Alp, R. Meyer, D. Sudfeld, E. Schuster, and W. Keune, *Phys. Rev. B* **76**, 195422 (2007).
 - ³² URL <http://www.sharcnet.ca>.